

MADMAC: A Test of Multispectral Airborne Imagery as a Farm Management Tool

M.S. Moran, T.R. Clarke, J. Qi and P.J. Pinter Jr.
 USDA-ARS U.S. Water Conservation Laboratory
 4331 E. Broadway Rd., Phoenix, Arizona 85040
 moran@tucson.ars.ag.gov

Abstract - An experiment called the Multispectral Airborne Demonstration at Maricopa Agricultural Center (MADMAC) was conducted to test the potential of airborne multispectral imagery for farm management application. Results presented here address image pre-processing algorithms, value-added products, and proposals for future direction.

I. INTRODUCTION

Airborne multispectral imagery can provide the fine spatial resolution, high temporal frequency and quick turnaround required for farm management applications. To test the potential for such applications, an experiment was conducted to acquire a season-long set of high-resolution (2-m pixel), multispectral videographic images over an agricultural area with detailed supporting ground measurements. This experiment was called the Multispectral Airborne Demonstration at the Maricopa Agricultural Center, or MADMAC.

Efforts were coordinated among scientists at three locations. Engineers at Utah State University provided the airborne remote sensing platform (flown at 2300 m and 1200 m), based on a system developed by ARS scientists in Weslaco, Texas. The video system consisted of three optical video cameras with green (0.545-0.555 μm), red (0.645-0.655 μm) and near-infrared (0.840-0.860 μm) filters, and a thermal scanning video filtered to 8.0-12.0 μm . Managers at the University of Arizona Maricopa Agricultural Center (MAC) provided their expertise and access to the 770 hectare research and demonstration farm located south of Phoenix, Arizona. Scientists from the U.S. Water Conservation Laboratory made a variety of ground measurements, including measurements of reflectance and temperature of large target areas, emissivity, leaf and soil temperature and reflectance, meteorological conditions, plant biomass and green leaf area index (GLAI), plant light interception and atmospheric optical depth. A total of fifteen overflights were made, spanning the cotton growing season from 12 April to 28 September, 1994. During each overpass, we made a detailed visual survey of MAC, recording 875 separate observations of crop type, estimated plant height, growth stage and percent crop cover, soil surface texture and dampness, and presence of insect damage, weeds or other anomalies.

Our initial research has focused on the development of

automated video image processing methods (to ensure rapid image turnaround), and the retrieval of pertinent crop and soil information from the multispectral images.

II. VIDEO IMAGE PRE-PROCESSING

Unprocessed airborne videographic images are characterized by distortions that occur due to unique camera optics and the attributes of the airborne platform. The interlacing of two video "fields" to produce each video frame results in a fractional, horizontal line shift of odd and even lines within the frame that blurs feature edges. The multi-camera system causes a misregistration of bands that varies throughout the flight due to varying aircraft elevation, motion and shutter. The wide field-of-view of most video cameras creates a non-uniformity in brightness across the imagery due to sun- and surface-induced bidirectional effects. Since most commercial video cameras are not calibrated to values of radiance, it is nearly impossible to use multitemporal images for monitoring changes in vegetation and soil conditions. We developed operational techniques to overcome these distortions and limitations.

A. Geometric Rectification

Horizontal line shifting, forming a zig-zag pattern at feature boundaries, varied sporadically in the MADMAC image frames, making a simple constant line shift insufficient (Figure 1). Furthermore, the average shift was typically less than a single pixel, requiring a fractional shift. We developed software that scanned the image line by line and, at feature boundaries, calculated the odd-line slopes and interline shifts. Analysis of the statistical mean and standard deviation for these net shifts were used to identify any shift anomalies, which were discarded from the calculation of the shift for that line. This was repeated for all sets of odd and even lines in the image, and using the same statistical mean and standard deviation calculations for the individual lines, outlying shifts were discarded and replaced with interpolated values. This algorithm provided an automated means for correcting continuously-changing, fractional line shifts that appear in videographic imagery (Mitchell et al., 1995).

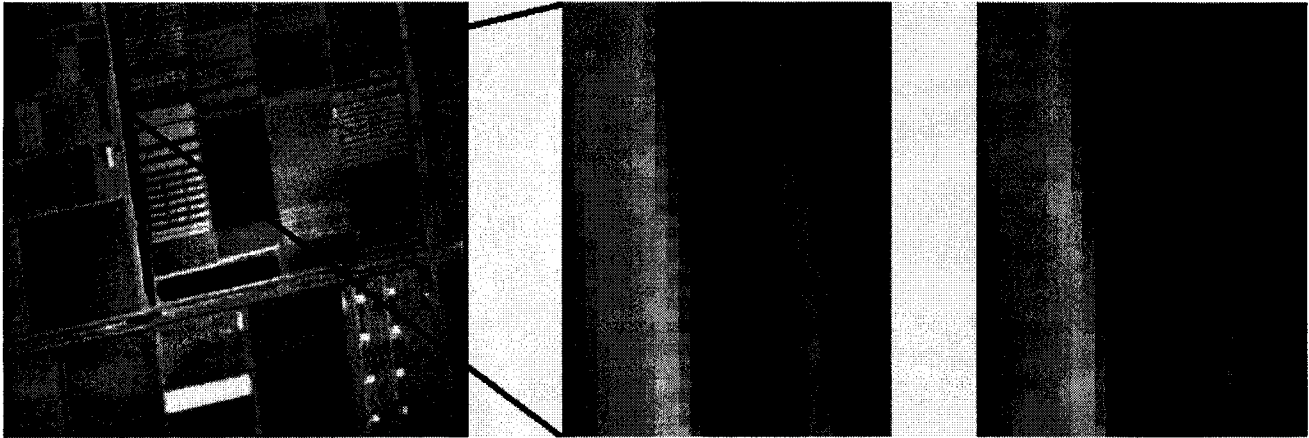


Figure 1. Image of MAC with line shift problems at feature edges. Middle and right images show feature edges before and after line shift correction.

Band-to-band misregistration, caused by misalignment of cameras and aircraft motion, is commonly corrected using automated image correlation techniques, where the alignment is determined by the location of the highest image correlation. This worked well for the red/green band registration at MAC because the images were positively correlated for all targets. However, the NIR band is both positively and negatively correlated with the red or green band, depending upon the feature. When an attempt was made to correlate the NIR with the green or red images, the positive and negative correlations for the different features began to add destructively, causing an erroneous shift. This problem was resolved by treating both images with a high pass filter to identify changes related to feature boundaries and then taking the absolute value of this change, thereby providing only positive correlations between bands (Figure 2). Application of this algorithm to MAC images resulted in exceptional band registration for all bands, including the NIR, with a failure rate of less than 2% and processing time of only 15 minutes for 80 sets of 3-band images (Mitchell et

al., 1995).

B. Normalization of Bidirectional Effect

Bidirectional effects are different from vignetting effects. Vignetting is associated with the optics of the sensor system and can be easily corrected with a camera-specific filtering function; whereas bidirectional effects are related to the surface optical properties, making correction more complex. Bidirectional effects in video images are due to the anisotropic nature of both vegetation and soil, and the different radiation levels associated with shaded and sunlit surfaces. The total field-of-view of the cameras used in MADMAC was $\pm 12^\circ$; with this configuration, we found that surface radiance of vegetated MAC fields varied by up to 24% due to bidirectional effects.

An automated procedure was proposed to normalize these effects, based on inversion of a Bidirectional Reflectance Distribution Function (BRDF) model. With multidirectional measurements of a single target provided by multiple video

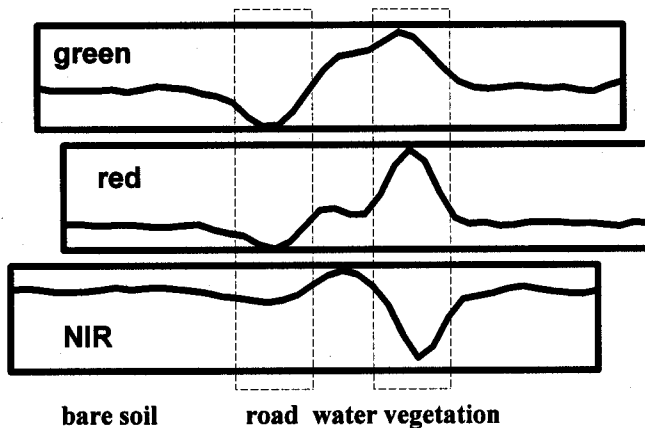


Fig. 2a. High pass feature correlations

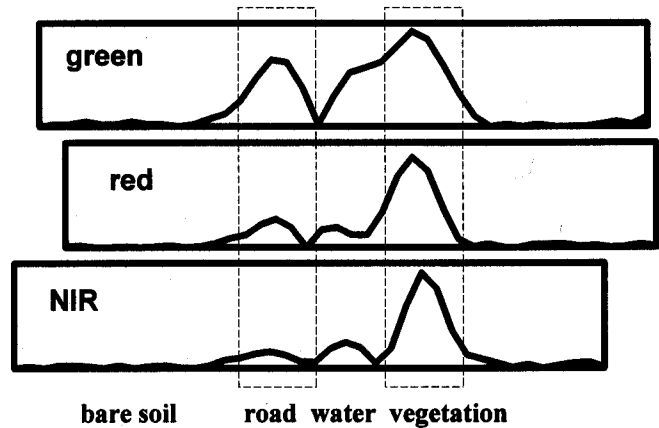


Fig. 2b. Absolute value feature correlations

frames, the BRDF model was inverted to produce model input parameters. These parameters were used to run the model and produce a set of coefficients for normalization of the bidirectional effect in the original image (Figure 3). To use this approach in practical operations, simultaneous multidirectional measurements are needed. Videographic imagery, with its fine spatial resolution and continuous frame acquisitions, provides such multidirectional measurements and, therefore, allows normalization of the bidirectional effects without prior knowledge about the surface properties (Qi et al., 1995).

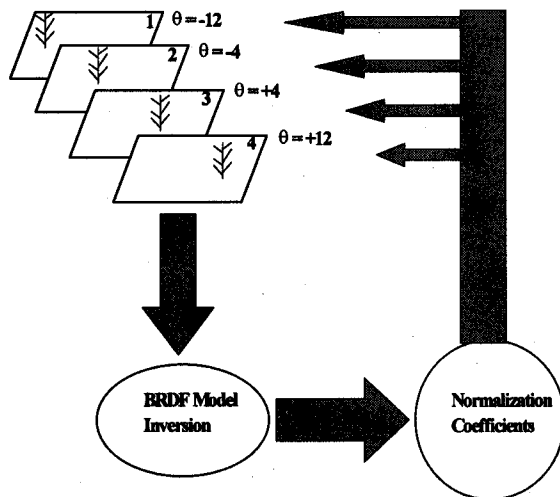


Figure 3. Procedures for correcting bidirectional effects on videographic imagery, where θ is the view angle of the sensor.

C. Reflectance and Temperature Retrieval

To conduct quantitative, multitemporal analysis for farm management applications, it was necessary to convert MADMAC digital video data into values of surface reflectance and temperature. We accomplished this with the deployment of large (8 m x 8 m) reflectance tarps of low (0.08) and high (0.64) reflectance (consistent over visible and NIR wavelengths) during every aircraft overpass (Teillet et al., 1987). After each flight, we retrieved the video digital numbers associated with the center of the reflectance tarps and computed a best fit between the surface reflectance of the tarps and the corresponding video digital number (setting the intercept to zero). This approach allows a camera-independent means for retrieval of reflectance factors from video images at any time of day, without making on-site measurements of atmospheric conditions. The results were validated with on-site measurements of surface reflectance in fallow and vegetated fields made with yoke-based radiometers. Care should be taken in applying this method

to avoid using pixels associated with tarp edges since these could be contaminated by atmospheric multiple scattering effects. We found that, for these 8 m x 8 m tarps with relatively clear-sky conditions, we needed 1-m resolution data to obtain an uncontaminated measurement in the center of the tarp.

To retrieve temperature from video digital numbers, we used another approach. The thermal video camera provided a conversion of digital number to temperature for each frame; however, it was still necessary to account for atmospheric attenuation and convert this "apparent" temperature to surface temperature. In an analysis of eight thermal images acquired at MAC in 1984, Moran (1990) found that the relation between apparent temperature and surface temperature was linear with a constant slope and an offset that varied with total atmospheric water vapor. Thus, the atmospheric correction of the MADMAC thermal images was accomplished by first computing apparent temperature based on sensor calibration. Then, a simple additive correction was computed based on the difference between an on-site measurement of surface temperature and the temperature of the same site measured by the airborne sensor. The results of this approach were validated by comparison of retrieved temperature with on-site measurements of temperature in fallow and vegetated fields.

III. VALUE-ADDED PRODUCTS

Initially, three algorithms were tested to retrieve pertinent crop and soil information from the multispectral images. The products were 1) a crop change map computed by subtracting one Vegetation Index (VI) image from a more recent one; 2) a Water Deficit Index (WDI) map computed from thermal and VI images to show actual to potential evaporation rates; and 3) a Crop Stress Index (CSI) map, which is a special application of the WDI concept to rank crop transpiration rates.

A. Crop Change Map

Discrimination of crop growth and plant status is generally accomplished by computing a ratio or linear combination of visible and near-infrared reflectance, such as the Soil-Adjusted Vegetation Index (Huete, 1988)

$$SAVI = (\rho_{NIR} - \rho_{Red}) / (\rho_{NIR} + \rho_{Red} + L)(1 + L), \quad (1)$$

where $L=0.5$, and ρ_{NIR} and ρ_{Red} are reflectance of the surface in the near-infrared (NIR) and red spectrum (respectively). Vegetation indices (VIs), such as SAVI, have been found to be sensitive to such vegetation parameters as green leaf area index (GLAI), fraction absorbed photosynthetically active radiation (fAPAR), and percent of the ground surface covered by green vegetation (V_g) (Jackson and Huete, 1991). By subtracting one SAVI map from the SAVI map of the preceding overflight, it is possible to map crop changes over

the period between flights. The result is a grey scale map where black indicates decreases in vegetation, grey indicates no change, and white indicates vegetation increases (Figure 4). This map gives the grower a visual method for comparing rates of change among fields with similar irrigation schedules or fertilizer applications, and thus, determining optimum management options.

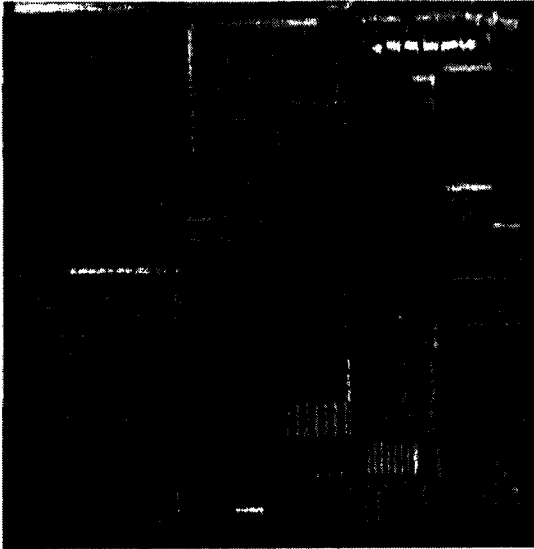


Figure 4. Map of crop change at MAC research farm. This map shows the difference of SAVI on 6 and 12 July 1994, where black indicates decreases in vegetation, white indicates increases, and grey indicates no change.

B. Water Deficit Index Map

Algorithms based on the difference between remotely-sensed surface temperature (T_s) and air temperature (T_a) have been developed to assess soil salinity, soil waterlogging, plant water potential and photosynthesis, as well as final crop yield (see reviews by Jackson, 1987; Pinter et al., 1979). The sensitivity of $T_s - T_a$ to plant and soil moisture conditions is related primarily to the heat loss associated with evaporation and transpiration (Idso et al., 1986). However, the sensitivity of $T_s - T_a$ to evapotranspiration rate (ET) is still confounded by variations in vegetation cover (V_c). Thus, attempts have been made to combine VI and $T_s - T_a$ in a single index related to the water status of the plants and soil in the field (Hatfield and Pinter, 1993). As the VI increases, the range of possible $T_s - T_a$ values for a given range of ET decreases, resulting in a trapezoidal Vegetation Index/Temperature (VIT) shape (Figure 5). Moran et al. (1994) proposed that the Penman-Monteith equation could be used to define the edges of the VIT trapezoid, thus allowing computation of a Water Deficit Index (WDI) defined by the ratio of AC/AB in Figure 5. This ratio is directly related to the ratio of actual to potential ET, where

$$WDI = 1 - (ET/ET_p), \quad (2)$$
 and $WDI=1$ when $ET=0$ and $WDI=0$ when $ET=ET_p$. The result is a grey scale map where bright shades indicate ET is close to zero and dark shades indicate ET is close to ET_p (Figure 6). The WDI has been found to be useful for such farm management applications as monitoring efficacy of irrigation applications and mapping soil moisture conditions (Moran, 1994).

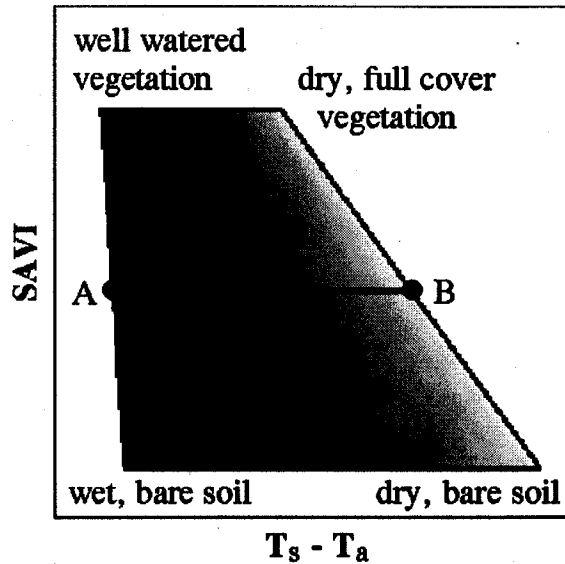


Figure 5. Water Deficit Index (WDI) Legend.

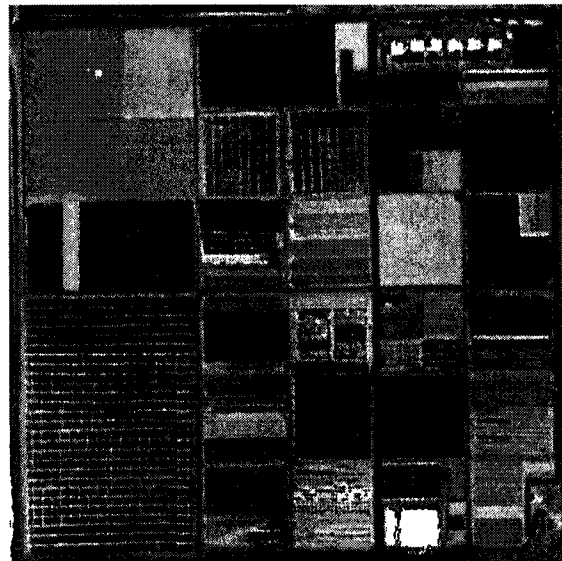


Figure 6. Water Deficit Index Map of MAC on 12 July 1994. WDI ranges from 0 to 1, where bright shades indicate $WDI=1$ ($ET=0$) and dark shades indicate $WDI=0$ ($ET=ET_p$). The bright white features in the upper right and lower right quadrants are roofs and water bodies, respectively. The small white square in the upper left quadrant is the 8 m x 8 m reflectance (0.64) tarp.

C. Crop Stress Index Map

A variation in the interpretation of the VIT trapezoid was proposed to accentuate differences in crop stress and compute a Crop Stress Index (CSI). In this interpretation, sections of the VIT trapezoid that were most likely *not* associated with crop stress were designated; that is:

- a wedge of the trapezoid close to the “cool” edge was associated with wet soil conditions;
- values below a designated threshold of VI were associated with bare soil conditions; and
- a wedge in the center of the trapezoid was associated with well-watered vegetation (Figure 7).

In the resultant map (Figure 8), pixels associated with these sections of the VIT trapezoid were colored black, and the remaining section of the trapezoid was colored with a grey scale ranging from dark to light associated with sufficiently-watered to dry vegetation, respectively (Clarke et al., 1994). This map of CSI could be interpreted by farmers for determining when to irrigate and how much water to apply, and identifying fields with insect infestation or other plant health problems.

IV. FUTURE DIRECTION

Future work will be focused on two concepts: 1) assimilation of infrequent, remotely-sensed information into physically-based simulation models to provide accurate, *daily* soil and crop information and 2) merging remotely-sensed information with a decision support system (DSS) to provide critical information for such farm management applications as irrigation scheduling, and chemical applications.

Infrequent but accurate measurements of remotely-sensed surface parameters (such as vegetation cover, soil moisture, evaporation rate and plant vigor) could be supplemented with daily simulated estimates of such parameters based on physical models and meteorological information (Figure 9). Operationally, an automated, numeric calibration procedure would be used to assimilate periodic remotely-sensed determinations of such parameters as plant green leaf area index (GLAI) and surface evaporation rate into a simple vegetation growth/soil water simulation model (e.g., Moran et al., 1995). Thus, the *high temporal frequency* of the simulation model would be combined with the *high spatial resolution and high accuracy* of the remotely-sensed data to provide daily, accurate maps of some surface parameters for effective resource management.

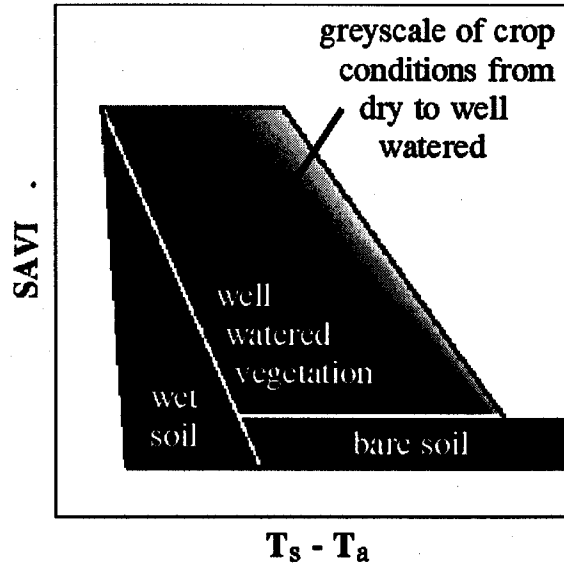


Figure 7. Crop Stress Index (CSI) Legend.

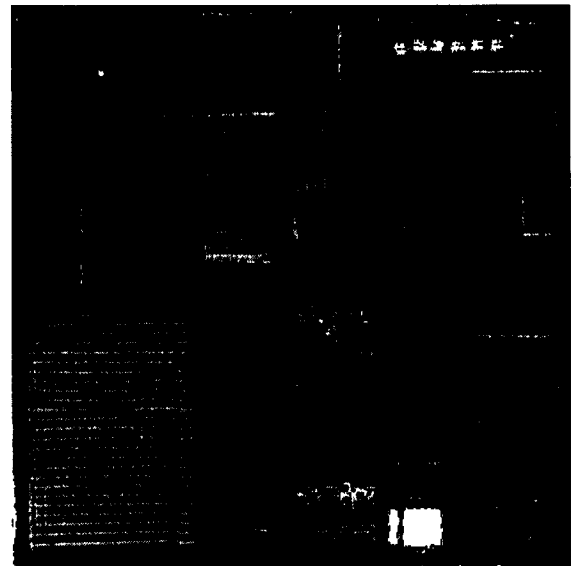


Figure 8. Crop Stress Index Map of MAC on 12 July 1994. Areas associated with wet soil, bare soil and well-watered crops are colored black; areas colored grey to white indicate vegetation conditions ranging from sufficiently-watered to dry, respectively.

To optimize the usefulness of remotely-sensed information for such farm management decisions as irrigation scheduling and chemical applications, it will be necessary to incorporate this information in a decision support system (DSS) such as DSS for Agrotechnology Transfer (DSSAT) (Hoogenboom et al., 1994). This would allow new possibilities (e.g., growth modeling and yield forecasting) for the application of multispectral data in site specific agricultural.

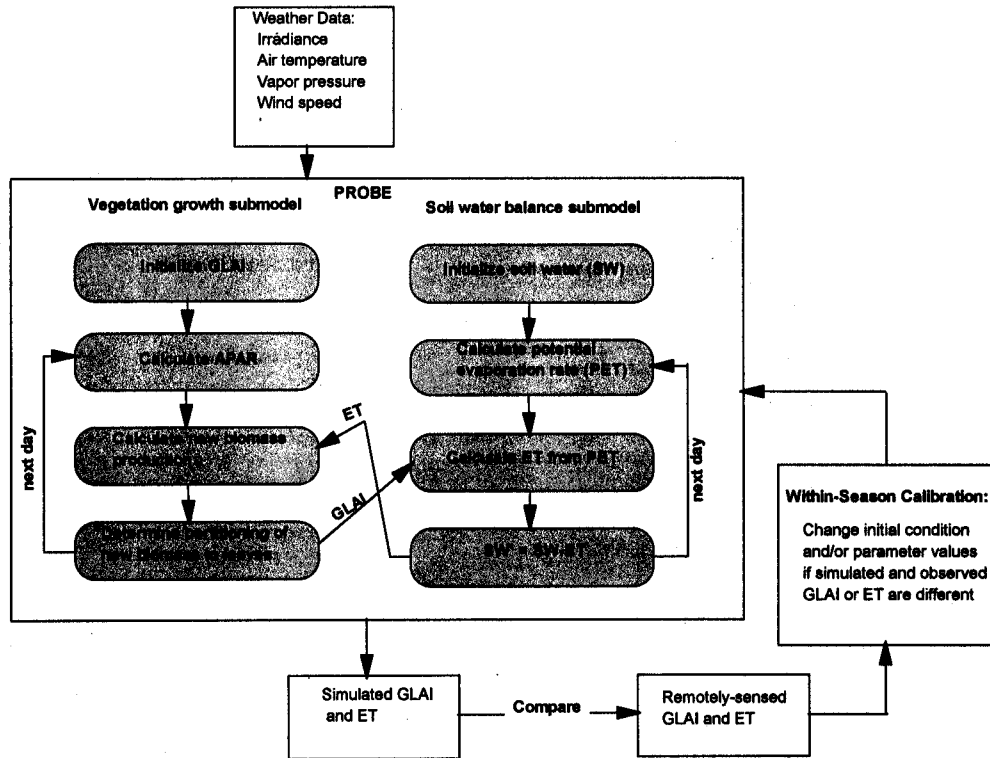


Figure 9. Assimilation of remotely-sensed information in a vegetation growth/water balance model with an automated, within-season calibration procedure (from Moran et al., 1995).

V. REFERENCES

- Clarke, T.R., M.S. Moran, Y. Inoue and A. Vidal (1994) Estimating crop water deficiency using the relation between surface minus air temperature and spectral vegetation index, *Proc. Sixth Intl. Symp. Phys. Meas. and Sign. in Rem. Sens.*, 17-21 January, Val d'Isere, France, p.1021-1028.
- Hatfield, J.L. and P.J. Pinter Jr. (1993) Remote sensing for crop protection, *Crop Protection* 12:403-413.
- Hoogenboom, G., J.W. Jones, L.A. Hunt, P.K. Thornton and G.Y. Tsuji (1994) An integrated decision support system for crop model applications, *Proc. ASAE*, Kansas City, 19-22 June, 94-3025:1-23.
- Huete, A.R. (1988) A soil-adjusted vegetation index (SAVI), *Rem. Sens. Environ.* 25:295-309.
- Idso, S.B., K.L. Clawson and M.G. Anderson (1986) Foliage temperature: effects of environmental factors with implications for plant water stress assessment and the CO₂/climate connection, *Water Res. Research* 22:1702-1716.
- Jackson, R.D. (1987) The Crop Water Stress Index: A Second Look, *Proc. Intl. Conf. on Meas. of Soil and Plant Water Status*, Utah State Univ., 6-10 July, Logan, UT.
- Jackson, R.D. and A.R. Huete (1991) Interpreting vegetation indices, *Prev. Veterin. Med.* 11:185-200.
- Mitchell, T.A., J. Qi, T.R. Clarke, M.S. Moran, C.M. Neale and R. Schowengerdt (1995) Geometric rectification of multi-temporal multi-band videographic imagery, *Proc. 15th Bien. Workshop on Color Photog. and Videog. in Res. Assessment*, Terre Haute, Ind., 1-3 May, p. 100-105.
- Moran, M.S. (1990) A satellite-based approach for evaluation of the spatial distribution of evapotranspiration from agricultural lands, *Ph.D. Dissertation*, Dept. of Soil and Water Science, Univ. of Ariz., Tucson, Az., pp. 223.
- Moran, M.S. (1994) Irrigation management in Arizona using satellites and airplanes, *Irrig. Sci.* 15:35-44.
- Moran, M.S., T.R. Clarke, Y. Inoue and A. Vidal (1994) Estimating crop water deficit using the relation between surface-air temperature and spectral vegetation index, *Rem. Sens. Environ.* 49:246-263.
- Moran, M.S., S.J. Maas and P.J. Pinter, Jr. (1995) Combining remote sensing and modeling for estimating surface evaporation and biomass production, *Rem. Sens. Reviews* 12:335-353.
- Pinter, P.J. Jr., M.E. Stanghellini, R.J. Reginato, S.B. Idso, A.D. Jenkins and R.D. Jackson (1979) Remote detection of biological stresses in plants with infrared thermometry, *Science* 205:585-587.
- Qi, J., T.A. Mitchell, M.S. Moran, P.J. Pinter Jr., T.R. Clarke, C.M. Neale, S. Sundararman, and R. Ahmed (1995) Normalization of bidirectional effect in videographic imagery, *Proc. 15th Bien. Workshop on Color Photog. and Videog. in Res. Assessment*, Terre Haute, Ind., 1-3 May, p. 77-86.
- Teillet, P.M., P.N. Slater, R.D. Jackson, G. Fedosejevs, and M.S. Moran (1987) Reflectance Measurements at White Sands, New Mexico, Using a Mobile Spectroscopy Laboratory, *Proc. 11th Canadian Symp. on Rem. Sens.*, Waterloo, Ontario, Canada, pp. 441-450.

VI. ACKNOWLEDGMENTS

We would like to thank Christopher Neale and his staff in the Dept. of Biol. and Irrig. Eng. at Utah State Univ.; Roy Rauschkolb, Bob Roth, Pat Murphree and MacD Hartman of the Univ. Ariz. Maricopa Agricultural Center; Steve Maas, USDA-ARS U.S. Cotton Research Station, Shafter, Cal.; and the many, hard-working technicians from USDA-ARS U.S. Water Conservation Lab.